Acoustic Signatures and Impedance Microstructure, Textural Scales, and Anisotropy of Kerogen-Rich Shale

Manika Prasad
Colorado School of Mines, Golden, CO 80401, USA
Tapan Mukerji
Stanford University, Stanford, CA 94305
M. Reinstädtler and W. Arnold
Fraunhofer Institute for Nondestructive Testing , D-66123 Saarbrücken, Germany

Abstract

A big challenge in studying organic rich shale is to predict its kerogen content and maturity from indirect observations. Kerogen maturation changes shale texture; for example, it generates microcracks and fractures in the matrix. Assessment of maturity from indirect measurements can be greatly enhanced by exploiting any existing correlations between physical properties, microstructure, and kerogen content. This paper shows how impedance microstructure of organic rich shale can be related to its maturity and elastic wave velocity.

Microstructural variations significantly affect seismic wave propagation. Traditional techniques for studying microstructure either give surface information or are limited in resolution. We have used results of scanning acoustic microscopy to analyze and map impedance microstructures in organic rich shale. We have also analyzed the acoustic images to quantify textural anisotropy and heterogeneity and relate these textural properties to acoustic wave propagation parameters of impedance at micrometer and centimeter scales. The acoustic and microstructural differences in shale from various stages of kerogen maturation (diagenesis, catagenesis, and metagenesis) show that:

1. Acoustic impedance of the shale matrix is related to its total organic content and to hydrogen index
2. Pyrite, a common accessory mineral, increases impedance of the altered areas as compared to the unaltered kerogen material
3. In high porosity shale, velocity is directly related to porosity. In low porosity shale, velocity is dependent on kerogen content
4. Textural heterogeneity, elastic impedance, velocity, and density increase with increasing shale maturity.

[Note: parts of this paper were published in two parts in the Acoustical Imaging Proceedings, 2005]

Introduction

One of the great challenges in exploiting kerogen-rich shale is to predict kerogen content and maturity from indirect observations. Because changes in shale texture and in hydrogen content are closely linked with kerogen maturity, their correlation with velocity, for example, would enhance methods for detection and exploration of kerogen rich shale. However, the intrinsic anisotropic texture of the shale and the close association of pyrite with kerogen make such a correlation difficult to establish. Microstructural characteristics of organic rich shale can give important insights on the maturation processes and on oil generation from such formations (Vernik and Nur, 1994). Attempts have been made to relate acoustic velocity and velocity anisotropy to the degree of kerogen maturity of the shales (Vernik and Nur, 1994; Vernik and Landis, 1996; Vernik and Liu, 1997). Chong and

Smith (1984) showed that as organic content of a rock increased, its physical properties were influenced and finally dominated by those of the organic materials. For example, organic matter containing a large proportion of aliphatically associated hydrogen tends to have lower density and to deform plastically under load, whereas organic matter with less hydrogen has higher density and lower plasticity. Lewan (1987) has documented microstructure changes observed in maturation during hydrous pyrolysis experiments. These studies have greatly improved our understanding of the ultrasonic properties and microstructure in kerogen rich shale.

Most of the above studies used optical and scanning electron microscopy methods to analyze kerogen shale microstructure. However, due to the opaque nature of the kerogen and the associated pyrite, such methods are rather difficult to implement. The present study was aimed at establishing a relation between elastic properties and kerogen microstructure and at understanding changes in elastic properties during maturation. For example, studies have shown that microgeometry, textural heterogeneity, and textural anisotropy have significant effects on the effective elastic properties of rocks. On the other hand, Prasad et al. (2002) have shown we can map textural changes with shale maturity with acoustic microscopy. We have aimed at establishing a relation between elastic properties and kerogen microstructure and at understanding changes in elastic properties during maturation.

We have revisited the ultrasonic data collected by Vernik and co-authors. In addition to optical microscopy, we used a comparatively new technique (scanning acoustic microscopy) to map the impedance microstructure of kerogen-rich shale. With this technique, in addition to the optical properties, we were able to map changes in elastic properties as the shale undergoes maturation. This paper reports results of acoustic characterization in samples belonging to various maturity grades and with different kerogen contents. Since microgeometry also plays an important role in the overall effective elastic properties of shale, characterizing and understanding the microgeometry, textures, scales, and textural anisotropy is important for better understanding the effect of microgeometry on effective elastic properties. A second aspect of this paper deals with characterizing and quantifying textural heterogeneity and anisotropy in the kerogen-rich shale and relating these properties to seismic properties. We use image analyses techniques to detect changes in texture and heterogeneity in the acoustic microscopy images at a micrometer scale and related them to ultrasonic measurements on a centimeter scale.

Methods and Materials

The acoustic images were made with an acoustic microscope and image analysis techniques are used to detect changes in texture and heterogeneity in these images.

Acoustic Microscopy (AM)

We used a non-destructive technique to map the impedance microstructure of kerogen-rich shale with a Scanning Acoustic Microscope (SAM). The C-scan surface images were made at 1 GHz. With this technique we could map changes in elastic properties as the shale undergoes maturation. A complete description of the application of scanning acoustic microscopy to petrophysics can be found in Prasad (2001) and Prasad et al. (2002). Here we describe only main principles. The basic principle is almost identical to that of reflection seismology. Images of surface and sub-surface microstructures are prepared on the basis of reflected acoustic waves – that is, on the impedance changes in the sample. Acoustic waves impacting on a sample are mode converted, partly transmitted into the sample, and partly reflected. The reflection coefficient and with it the signal intensity received by the transducer are determined by the elastic constants of the material. We study changes in acoustic impedance in the sample that influence wave reflection characteristics by mapping the reflected waves.

In this paper, we present AM results of kerogen-rich shale using a high frequency (0.2 – 2 GHz) acoustic microscope. This mi-

croscope operates in reflection mode. The depth of penetration and resolution of microstructural features depend on the operating frequency. The 1 GHz high frequency lens was used for high resolution about 1 µm with a scan area of 1x1 mm. At high (GHz range) frequency, design and curvature of the high frequency acoustic lenses are optimized to achieve a high sensitivity to surface acoustic (Rayleigh) waves. This design allows us to map microstructural features from the interference patterns between normally reflected longitudinal waves and the Rayleigh waves (Briggs, 1992).

In this paper, we shall discuss impedance variations on the basis of C-scans. These X-Y scans of surface and sub-surface features can be used to study impedance changes in the sample. In the simplest form, the acoustic images are used to study qualitative changes in impedance from the color coding, without information on whether the change is positive or negative. Hirsekorn and Pangraz (1994) have reported a method of calibrating the gray scale output of SAM with materials of known impedance. Expected impedance variations in rocks lie between 1.5 km/s*g/cc (for water) and about 30 km/s*g/cc (for olivine). Impedance variations in an unknown sample can be inferred from these "calibrated" gray scales provided that the instrument settings remain unchanged. This method assumes minimal instrumental drift. However, approximately 10-15% error is to be expected, especially if calibrations are not performed on a regular basis. The error is enhanced if the sample surface has topography.

The gray level in the shale impedance images changes from 0 (= black, low impedance) to 255 (= white, high impedance). The materials used for this calibration varied in impedance from 1.5 km/s*g/cc (water) to 25 km/s*g/cc (metallic glass). Impedance values were evaluated using a linear fit between the gray values measured and the reflection coefficient for each reference.

Image Processing: Statistical descriptions of heterogeneity and textures

The heterogeneity was quantified by the coefficient of variation (CV) of the image pixel values given by the ratio of the standard deviation to the mean of the image pixel values. We quantified textures using textures spatial autocorrelation functions R(m,n) and a Fourier transform based autocorrelation estimation (see detailed procedure in Mukerji and Prasad, 2007). In the equations given below, I(x,y) denotes the image intensity at pixel (x,y). The mean intensity is denoted by mean{I(x,y)} and a 2-d Fourier transform of the image I(x,y) is denoted by $\hat{I}(k_x,k_y)$ where k_x, k_y are the spatial wavenumbers in the Fourier domain. The power spectrum S is obtained by multiplying $\hat{I}$ with its complex conjugate $\hat{I}^*$. Finally the 2-d ACF R is obtained by taking the inverse Fourier transform of S. The example in Figure 1 shows how a smoothly varying image has a broad, slowly decaying autocorrelation function. In contrast a rough "salt-and-pepper" image has a very narrow spiky autocorrelation function.

CV = std. dev{I(x,y)} / mean{I(x,y)}

$$R(m,n) = E\{[I(x,y) - m_I][I(x+m, y+n) - m_I]\}$$

$$\hat{I}(k_x,k_y) = \iint I(x,y)\exp\{-i(xk_x + yk_y)\}dxdy$$

$$S(k_x,k_y) = \hat{I} \bullet \hat{I}^*$$

To analyze the kerogen shales, we first used a calibration function to convert color-coded image intensity values to elastic impedances. We then computed radial profiles of the autocorrelation function (ACF) along azimuths ranging from 0^o to 180^o and the correlation length at each azimuth. The correlation length is the lag value where the correlation function falls to 1/e of its maximum value at zero lag. The textural anisotropy, quantified by the anisotropy ratio (AR), is a measure of the ratio between the maximum and minimum correlation lengths obtained over all azimuths (see Figure 2). Textures were also analyzed using singular value decomposition (SVD) of the images (Figure 1). The spectrum of singular values shows different decay behavior for different textures.

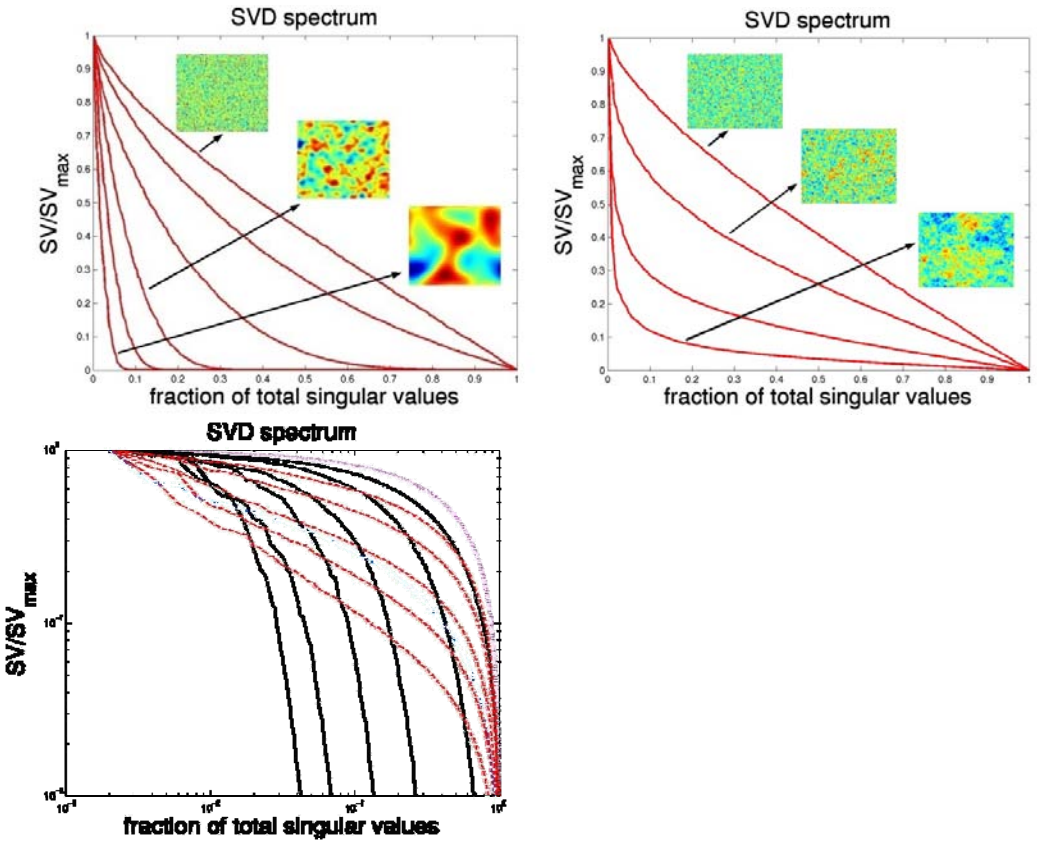

Figure 1: Singular value spectrum shows distinctive behavior for images with Gaussian spatial correlation (top left) versus fractal images (top right). In the bottom figure the black lines with a rapid fall off in singular value corresponds to images with Gaussian autocorrelation, while the dotted red lines correspond to SVD spectra of fractal images.

Samples Used

The samples used in this study belonged to the Bakken, Bazhenov, Monterey, Woodford, Niobrara, Lockatong and North Sea formations with varying degrees of maturation and kerogen content. Of these, eight samples were chosen for the acoustic microscopy study. Physical properties of the subset of eight samples are given in Table 1 (from Vernik and Liu, 1997).

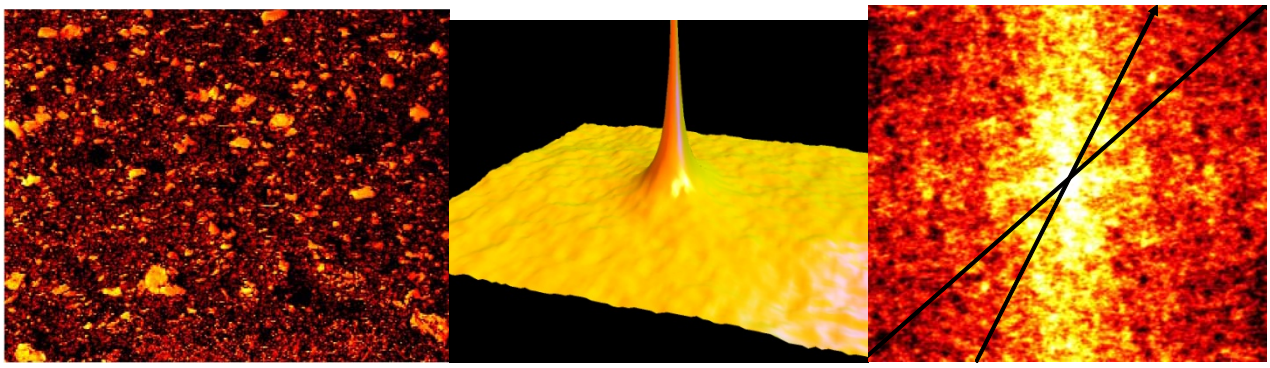

Figure 2: SAM image (a) and its corresponding 2-D autocorrelation function (ACF) (b). The result of computing radial profiles of the 2-D autocorrelation function along azimuths (as shown in c) by interpolation along the different directions (black lines). The correlation length was estimated at each azimuth. The peak is the autocorrelation at zero lag distance (maximum). It decays away on all sides with increasing lag with the rate of decay being a quantitative measure of texture.

Table 1: Properties of the kerogen rich shale samples used in this study (from Vernik and Liu, 1997). Phi = fractional porosity, TOC = total organic content in %, HI = hydrogen index in H (mg) / OC (g), KC = kerogen content.

Formation	Porosity	TOC	HI	KC	Maturity
Bakken	0.007	20.1	584	0.5	II
Woodford	0.008	6.6	582	0.207	II
Gaviota	0.288	7.9	572	0.155	II
Bakken	0.007	12.1	436	0.323	III
Bazhenov	0.032	4.7	422	0.137	III (?)
Bazhenov	0.02	2.8	288	0.085	IVa
Bakken	0.011	9.8	161	0.251	IV
Woodford	0.008	8.9	40	0.247	V

The Bakken, Bazhenov, and Woodford shale samples have low porosity; Bazhenov shale was also rich in clay content; and Gaviota shale was an outcrop sample with very high porosity. We have used velocity data at high pressure (60 MPa) to eliminate the effects of microcracks. The impedance microstructural analyses were combined with optical microscopy results of the same samples. The spatial resolution of both acoustic and optical microscopes is about 1 µm and therefore comparable.

Results

Analyses of Ultrasonic data

We first reevaluated the ultrasonic and physical property data to differentiate between kerogen and porosity effects on the elastic properties. Our analyses show that porosity effects dominate velocity variations in high porosity shale, whereas in low porosity rocks, velocity correlates with kerogen content. This effect is seen in Figure 3, where P-wave velocity in the high porosity shale is better correlated with porosity (Figure 3a); in the low porosity shale it is better correlated with maturity and kerogen content (Figure 3b). Correlation between Vp and HI is very high (Figure 3c) when we constrain the data by formation. Figure 3c shows data for Bakken shale only. Vp decreases with increasing HI and the difference between Vp in the fast and slow directions seems to be constant over the entire HI range.

Impedance microstructure

Impedance microstructure of the samples differed considerably. Acoustic micrographs (1 GHz C-scan surface images) of the Bakken shale series samples are shown in Figures 4 – 6 with increasing grades of maturity. The images illustrate differences in impedance microstructure between shale of varying grades of maturity ranging from II (Figures 4-5) through III (Figure 6) and IV (Figure 7) from the Bakken formation. The low impedance (less than 7.5) is masked by red color. The immature shale is exemplified by connectivity in the kerogen fabric. Figure 4 shows the C-scans in a maturity stage II Bakken shale at different magnifications; from 1 mm (right) to an expanded view of 62.5 µm (left). Impedance measurements in the matrix, in the higher impedance grains and average impedance of the entire image are also given in red numbers. The sample has very low impedance and a fine-grained texture. The aligned texture is due to “wispy”, short, elongated and partly connected carbonate grains.

The wispy microstructure gives the appearance of a double image in these samples. A detailed image of such a “wisp” texture is shown in Figure 5. This feature is remarkably similar to the parallel stacks of kerogen nuclei mapped by SEM (Tissot and Welte, 1978). The wispy nature in the impedance microstructure appears to dominate mainly in immature shale. According to Tissot and Welte (1978), the kerogen occurs as stacks of kerogen nuclei. These stacks are randomly distributed in immature kerogen. As the kerogen matures, the stacks get more organized and become aligned parallel to one another. However, the parallel texture observed in the C-scans is much larger (µm scale) than the nuclei stacks (Angstrom scale). It appears to be in the carbonate grains rather than in the kerogen, and was observed only in shale with low maturity.

Figure 6 shows some representative C-scans in the maturity stage III Bakken shale at different magnifications; from 1 mm (right) to an expanded view of 200 µm (middle).

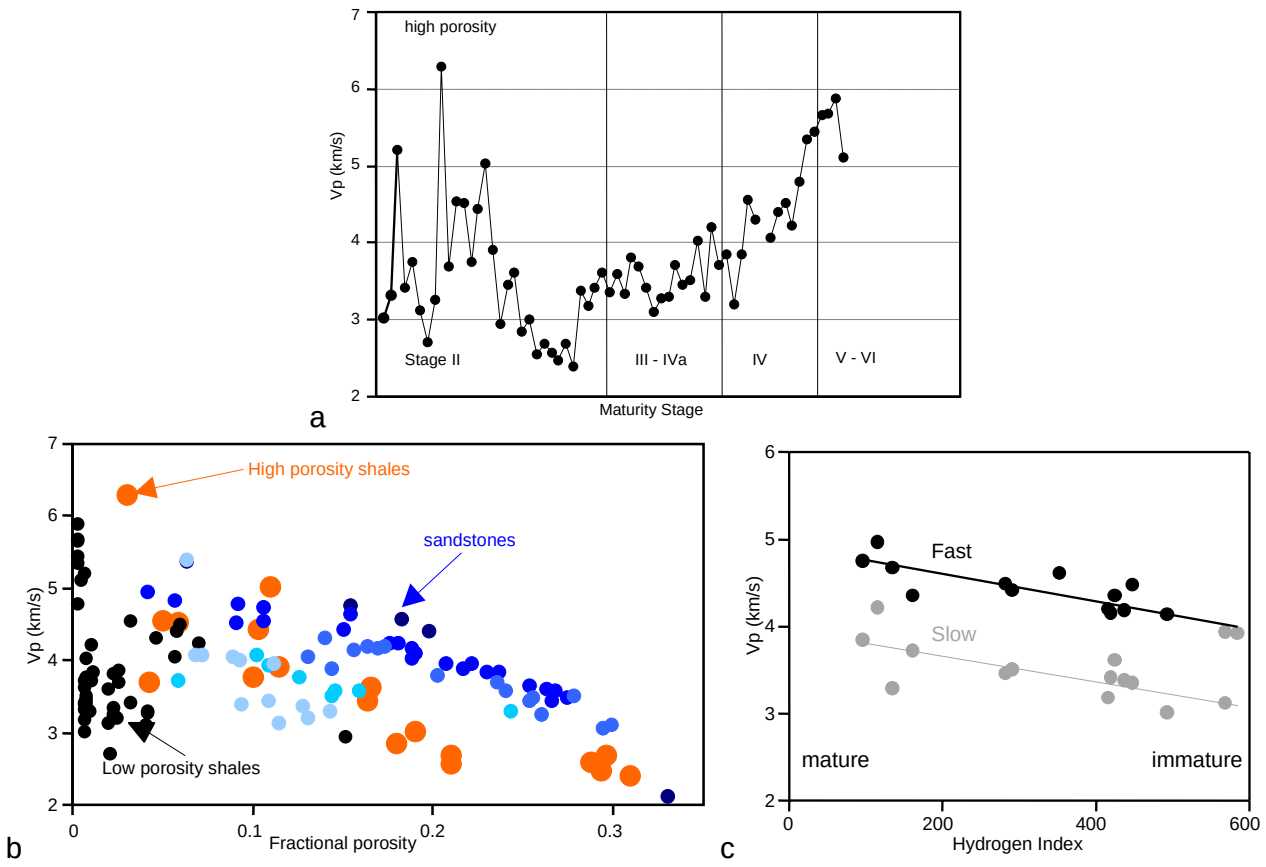

Figure 3: Correlation between Vp and maturity stage (a), porosity (b), and Hydrogen Index (c).

a. Vp increases with increasing maturity in direct relation with the overall increase in acoustic impedance on a micron scale observed in the acoustic micrographs.

b. Correlation between Vp and porosity in high (solid red symbols) and in low porosity kerogen shale (solid black symbols). Han's data for shaly sandstones (Han et al., 1986) are also plotted. Varying blue shades mark increasing clay content. High-porosity kerogen shale lies on the same trend as the sandstone with highest clay content, whereas the low porosity kerogen shale has lower velocity.

c. Vp variations with Hydrogen Index (HI) for Bakken shale only. Correlation between Vp and HI is high when data are constrained by formation. Vp decreases with increasing HI and the difference between Vp in the fast and slow directions seems to be constant over the entire HI range.

Impedance measurements in the matrix, in the higher impedance grains, and average impedance of the entire image were also measured. The impedance microstructure shows a network of higher impedance material than the matrix. The impedance appears to be increasing as compared to the grade II Bakken shale from Figure 4.

Figures 7 and 8 show C-scans of Bakken shale with maturity stages IV and V, respectively. As before, impedance measurements in the matrix, higher impedance grains, and average impedance of the entire image are presented. The impedance is higher than the grade II maturity shale in Figure 2. Furthermore, there appear to be a larger number of coarse grains in this mature shale as compared to the maturity stage II shale in Figure 4.

From the different maturity shale samples examined in this study, we find following major changes in the impedance microstructural images:

- Increase in impedance as maturity progresses
- Increase in grain size and in the number of coarse grains in mature shale

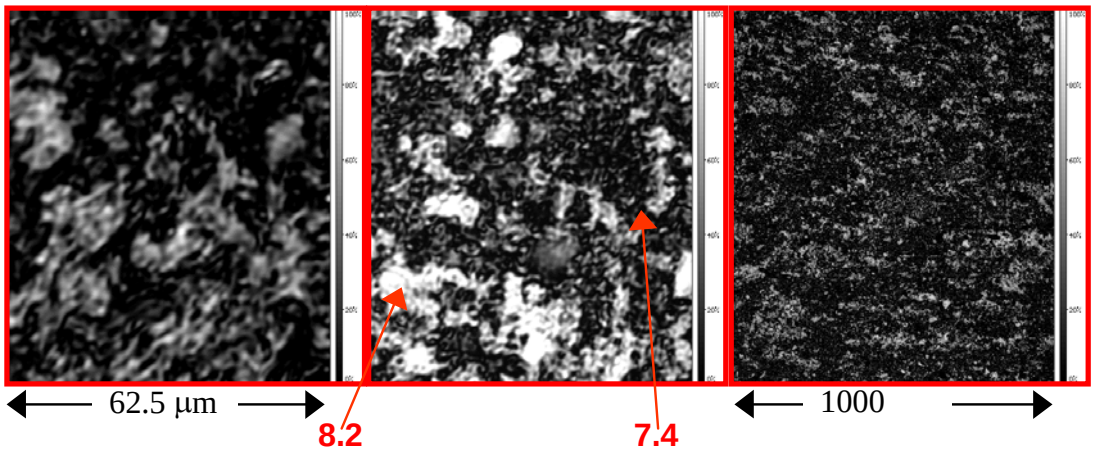

Figure 4: Acoustic images of Bakken shale of maturity stage II. Arrows mark position of measured impedance values (red numbers). The fine-grained matrix and grains show very low impedance changes. The aligned texture observed in the entire matrix is due to aligned, partially connected, elongated grains (ca. 20 mm).

- Distribution of kerogen and of the grains undergoes major change during maturation. The more or less connected kerogen matrix with higher impedance grains dispersed within it in the immature stage gives way to a grain supported framework containing kerogen after maturation. Also, there is a significant increase in the grain size with maturation.
- Parallel to sub-parallel kerogen filled cracks are more common in mature shale.

Microstructure variations with maturity:

A comparison of the textural variations with maturity gave some important insights in the process of kerogen maturation and its

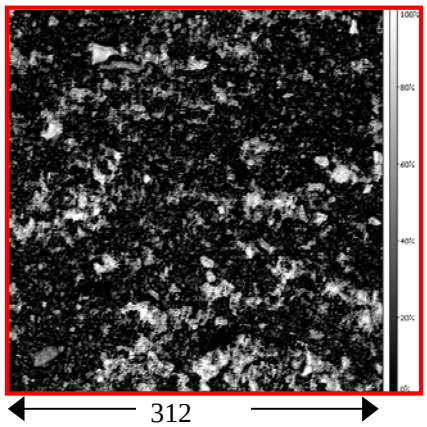

Figure 5: Acoustic images of a Bakken shale (8036 ft) showing aligned "wisps" of similar, high impedance materials. Texturally, these resemble the stacks of kerogen nuclei reported by Tissot and Welte (1978), although these wisps are much larger than the kerogen nuclei stacks.

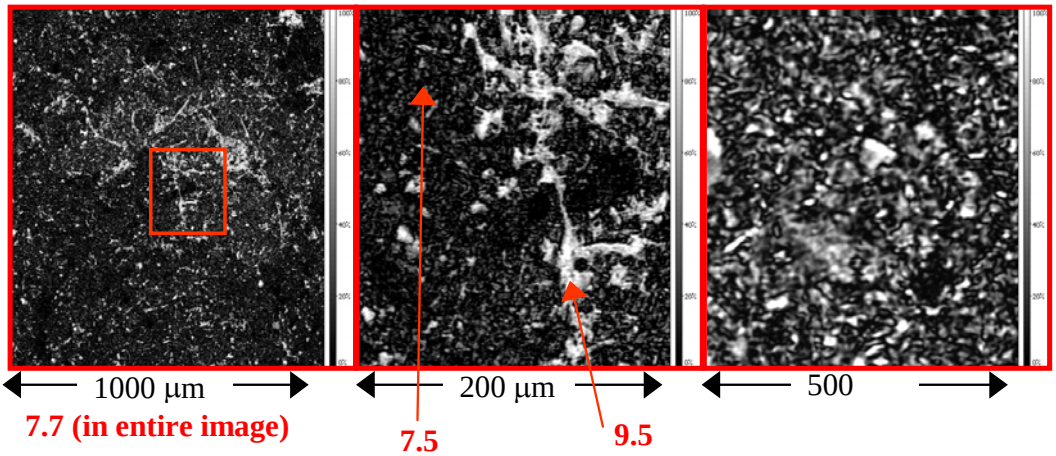

Figure 6: Acoustic images of Bakken shale of maturity stage III. Arrows mark position of measured impedance values (red numbers). Fine-grained matrix and grains show low impedance changes. Grains are elongated and connected by bridge-like growths that span very low impedance kerogen filled cracks.

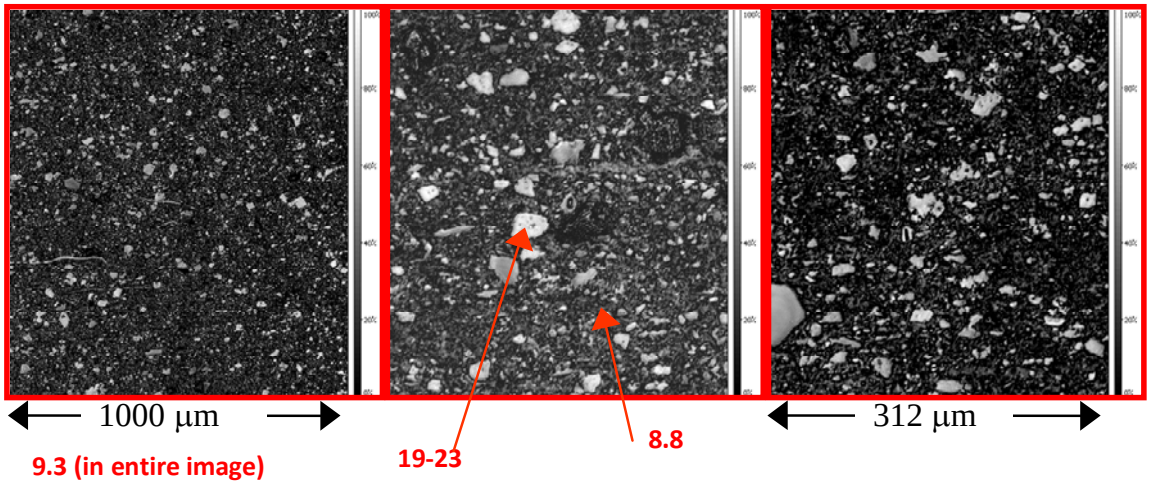

Figure 7. Acoustic images of a Bakken shale of maturity stage IV. Arrows mark position of measured impedance values (red numbers). The matrix and grains show higher impedance change, grains are coarser, and the overall impedance is higher than in the lower maturity shale of same formation. Sub-horizontal kerogen filled cracks with very low impedance are common.

effects on texture. There is a significant difference in texture with maturity (Figure 9 of two mature and two immature shale samples from the Bakken formations). In the images, the kerogen is coded as red (lowest impedance). Using this color code, it becomes apparent that kerogen is load bearing in immature shale and that it forms a connected network. In the mature shale, the kerogen appears dispersed in the matrix, and the grains are load-bearing. This characteristic has important effects on the velocity and on the pressure dependence of the velocity in the different shale types. In Figure 3, velocity decreased with decreasing kerogen content.

The change in impedance with maturity is shown in Figure 10. The acoustic impedance of the microstructural image is plotted against Hydrogen Index for all samples. An inverse linear relation is observed that is similar to the inverse linear relation between velocity and kerogen content (Figure 3). From the AM images (Figures 4 – 7), acoustic velocity measurements (Figure 3), and the relation between Hydrogen Index and microstructural impedance (Figure 10), a relation can be established between the changes in bulk acoustic and microstructural impedance properties.

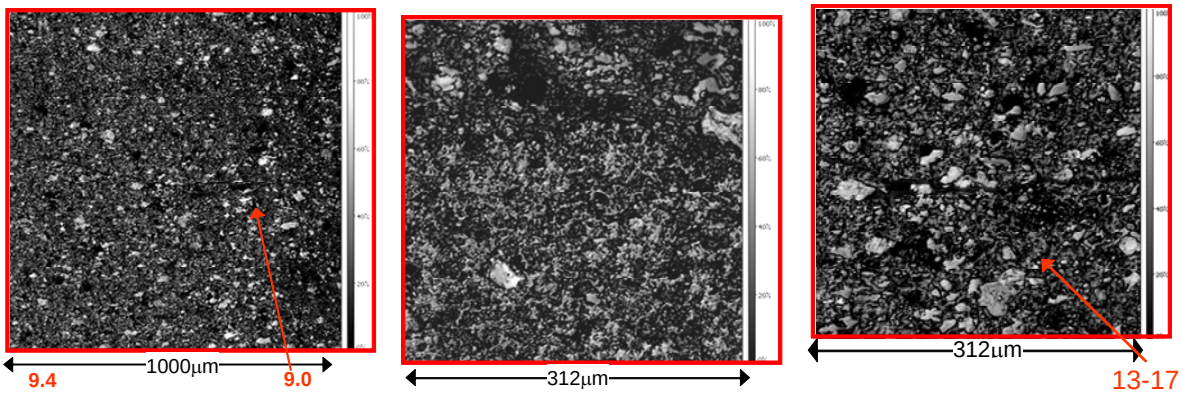

Figure 8: Acoustic images of a Bakken shale of maturity stage V. Arrows mark position of measured impedance values (red numbers). The matrix and grains show higher impedance change, grains are coarser, and the overall impedance is higher than in the lower maturity shale of same formation. Sub-horizontal kerogen filled cracks with very low impedance are common.

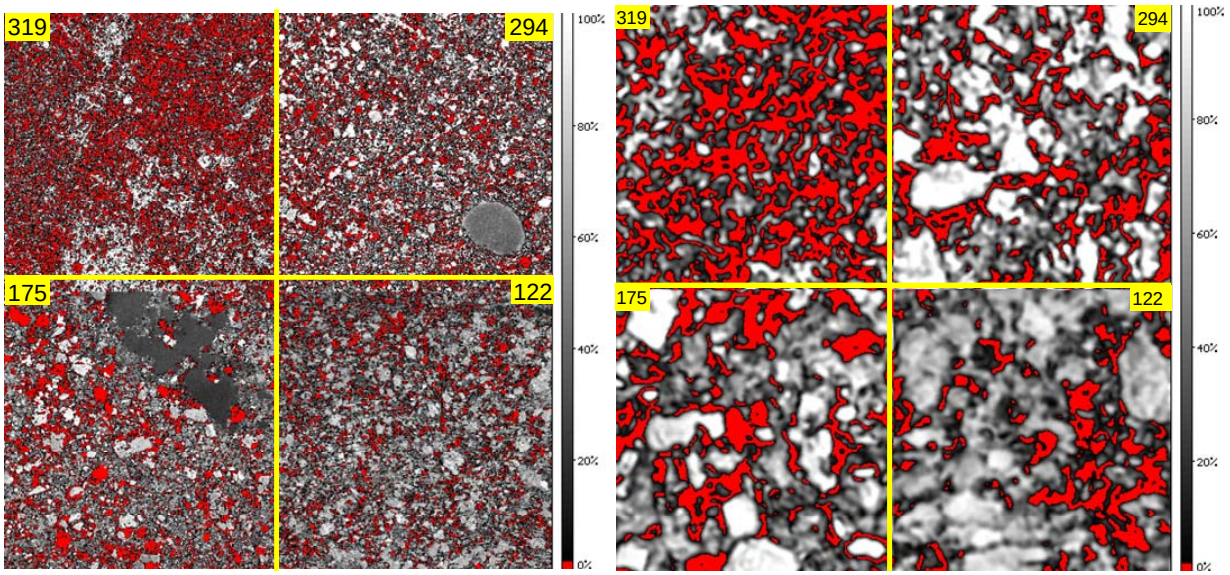

Figure 9: Impedance microstructure in the Bakken formation. The numbers show Hydrogen Index in each shale sample. A decreasing HI number denotes increasing maturity. The color code is chosen such that the lowest impedance is red. Note change in texture (decrease in red color) from immature (HI = 319) to mature shales (HI – 122). The scale on the left images is 1mm x 1mm and in the images on the right it is 62μm x 62μm.

Textural Analysis

We analyzed variability within images by processing different subsections of the same image, making sure to sample subsections much larger than the mean correlation length to obtain valid statistics. SVD spectra of the images are distinctly different from SVD spectra of synthetic images with Gaussian autocorrelation. They show more resemblance to SVD spectra of fractal images.

We quantified textural properties using statistical descriptions of heterogeneity and textures. The Coefficient of Variation (CV) was used to describe textural heterogeneity, the Anisotropy Ratio (AR) to describe textural anisotropy, and the Mean Correlation

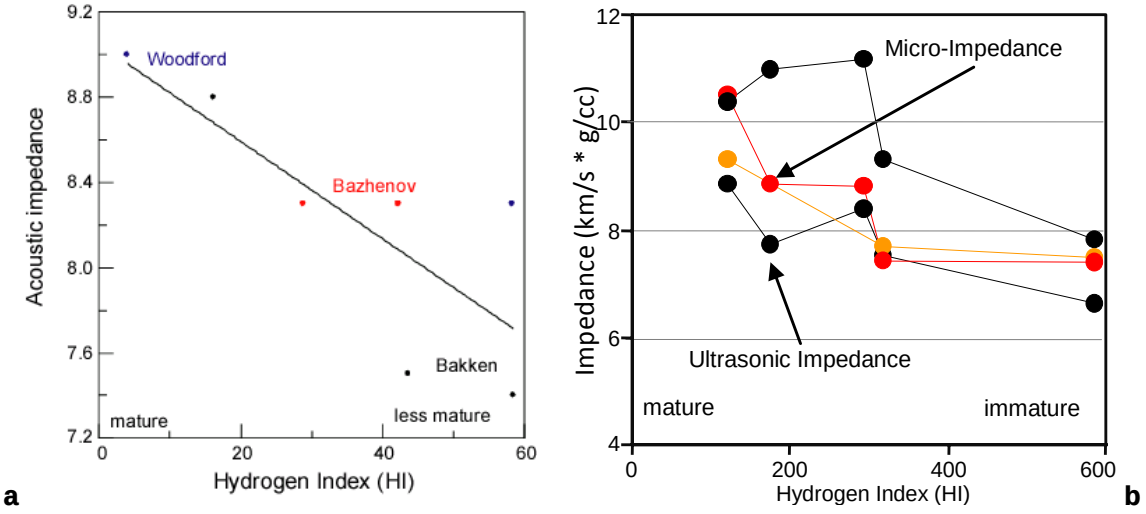

Figure 10: Correlation between Hydrogen Index (HI) and Acoustic Impedance measured with acoustic microscopy. There is a correlation between these properties measured at two different scales. However, the relation is masked by sample heterogeneity (a). This correlation becomes better if we constrain the samples to one formation (b)

Length to quantify textural scale in the images. Note that the presence of large-sized heterogeneities gives rise to longer correlation lengths. If there is a large impedance contrast in the heterogeneities, then high values of CV are calculated, and a systematic changes in texture with azimuth leads to a directional dependence of ACF. Thus, the three properties of CV, AR, and mean Correlation Length together allow us to measure and compare the changes in shale texture with maturation.

The results of texture analyses are shown in Figures 11 – 13. Figure 11 shows the estimated autocorrelation function and the azimuthal profiles. The impedance variation ranged from about 7% to 12%, whereas the mean correlation length ranged from 2 to 4.5 microns (Figure 11). In general, the textural anisotropy (AR) increased with increasing heterogeneity (CV), as seen in Figure 12. Mean correlation length decreases as textural heterogeneity (CV) increases showing that more mature (and deeper) samples have larger heterogeneities with higher contrast. Textural anisotropy (AR) increases with increasing correlation length. With depth (= maturity), textural anisotropy

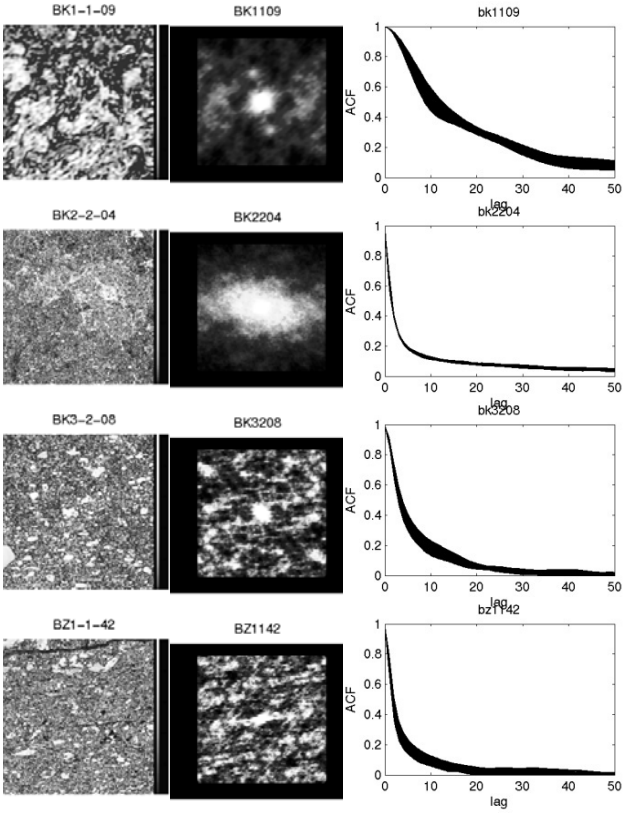

Figure 11a: Left: Acoustic Microscopy images, Middle: 2-D spatial autocorrelation of SAM images of varying maturities from the Bakken (BK), and Bazhenov (BZ) formations. Right: Azimuthal profiles of the corresponding autocorrelation function from 0 to 180 degrees. The correlation length at each azimuth is called the lag value where the correlation function falls to 1/e of its maximum value at zero lag. The ratio between maximum and minimum correlation lengths obtained over all azimuths gives a measure of the anisotropy. A larger spread of ACF with azimuth (such as in BK3208) indicates higher anisotropy.

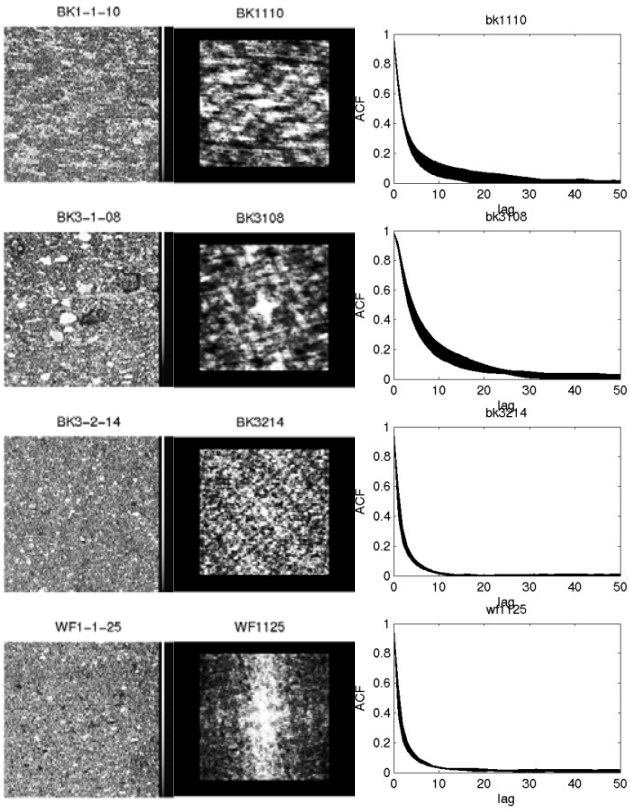

Figure 11b: Left: Acoustic Microscopy images, Middle: 2-D spatial autocorrelation of SAM images of varying maturities from the Bakken (BK) and Woodford (WF) formations. Right: Azimuthal profiles of the corresponding autocorrelation function from 0 to 180 degrees. The correlation length at each azimuth is called the lag value where the correlation function falls to 1/e of its maximum value at zero lag. The ratio between maximum and minimum correlation lengths obtained over all azimuths gives a measure of the anisotropy. A larger spread of ACF with azimuth (such as in BK1110) indicates higher anisotropy.

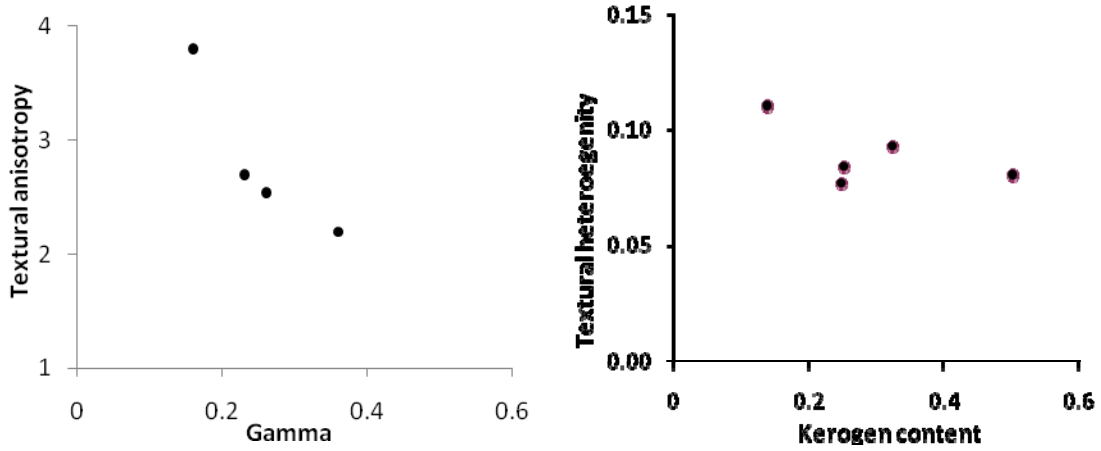

Figure 12: Left: Correlation between textural anisotropy from Acoustic Microscopy Images and the Thomsen anisotropy parameter γ from ultrasonic experiments. Right: Correlation between textural anisotropy from SAM images of varying maturities from the Bakken (BK) formation and their kerogen content.

increase is lower whereas the mean correlation length increase is larger, thus, deeper samples have lower anisotropy but larger heterogeneities.

Conclusions

Our study of the different maturity shale samples shows the following major differences in the impedance microstructure and in elastic properties:

- There is a inverse linear relation between velocity and kerogen content in shale with low porosity
- In high porosity shale, velocity is dependent on porosity
- Overall impedance of the sample increases as maturity progresses
- Grain size increases with maturity
- Distribution of kerogen and grains undergo major change as the maturity progresses. In immature shale, kerogen forms a connected matrix with higher impedance grains dispersed in this ma-

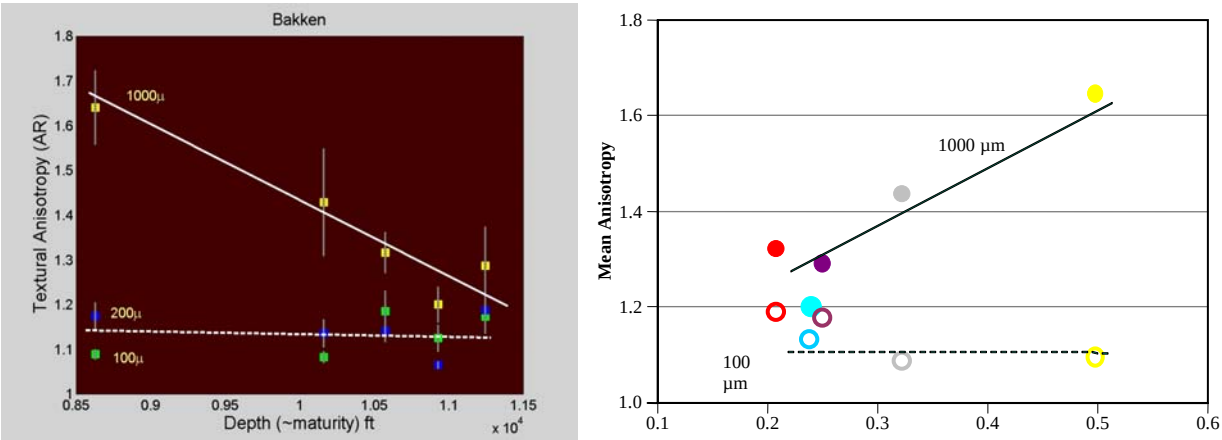

Figure 13: Left: Correlation between textural anisotropy from image analysis and depth. Right: Correlation between mean textural anisotropy from image analysis and kerogen content. The figures show that scale is important when considering textural parameters – there is a good correlation between kerogen content (and maturity) and textural parameters derives from images at 1000μm, but the textural anisotropy at the fine scale (100m images) does not show any trend with depth or kerogen content.

trix. In mature shale, there is a significant increase in the number of coarse grains. The grains form a framework and kerogen fragments are distributed within this frame.

- Bedding-parallel kerogen-filled cracks are more common in mature shale. In addition to layering, the texture is characterized by aligned kerogen-filled cracks causing acoustic anisotropy.

Using image analyses techniques, we could further quantify the impedance textures and relate them to ultrasonic seismic properties:

- Coefficient of variation (CV) (measuring impedance heterogeneity) ranges from 7% to about 12%.
- The mean correlation length tends to increase with increasing heterogeneity.
- Textural heterogeneity, elastic impedance, velocity, and density increase with increasing shale maturity.
- The textural spatial correlation length varies with direction.
- Textural anisotropy (AR) ranges from 10% - 70% and tends to decrease with increasing depth and maturity.

Acknowledgements

We thank the Fraunhofer Institute for Nondestructive Testing (IZfP) for use of AM facilities, Lev Vernik for suggesting to investigate organic rich shales, DHI/Fluids consortium at CSM and the SRB Project at Stanford for support. This work was partly supported by NSF (grant number EAR-0074330) and Petroleum Research Funds (grant number PRF#43596-AC8).

References

Briggs, G. A. D., 1992, Acoustic Microscopy: Monographs on the Physics and Chemistry of Materials, 47, Oxford Science Publications, 325 p.

Chong, K. P. and J. W. Smith, eds., 1984, Mechanics of Oil Shale: London, Elsevier Applied Science Publishers, 603p.

Han, D., A. Nur, and F. D. Morgan, 1986, Effect of porosity and clay content on wave velocities of sandstones: Geophysics, v. 51, p. 2093-2107.

Hirsekorn, S. and S. Pangraz, 1994, Materials characterization with the acoustic microscope: Applied Physics Letters, v. 64, p. 1632-1634.

Lewan, M. D., 1987, Petrographic study of primary petroleum migration in the Woodford Shale and related rock units, in Migration of hydrocarbons in sedimentary basins, in ed. B. Doligez, IFP Exploration Research Conference, 45, p. 113-130.

Mukerji, T. and M. Prasad, 2007, Image processing of acoustic microscopy data to estimate textural scales and anisotropy in shales, in International Symposium on Acoustical Imaging and Michael P. André. Acoustical Imaging 26: Dordrecht, Springer, p. 21-29.

Prasad, M., 2001, Mapping impedance microstructures in rocks with acoustic microscopy: The Leading Edge, v. 20, #2, p. 172-179.

Prasad, M., M. Reinstaedtler, A. Nur, and A. Walter, 2002, Quantitative Acoustic Microscopy: Application to petrophysical study of reservoir rocks: Acoustical Imaging, v. 26, p. 493-502.

Tissot, B. P. and D. H. Welte, 1978, Petroleum formation and occurrence: Springer Verlag, New York, 538 p.

Vernik, L. and C. Landis, 1996, Elastic anisotropy of source rocks: Implications for hydrocarbon generation and primary migration: AAPG Bulletin, v. 80, p. 531-544.

Vernik, L. and X. Liu, 1997, Velocity anisotropy in shales: A petrophysical study: Geophysics, v. 62, no. 2, p. 521-532.

Vernik L. and A. Nur, 1994, Ultrasonic velocity and anisotropy of hydrocarbon source rocks: Geophysics, v. 57, no. 5, p. 727-735.